
















































The Day-long, Repeating GRB 250702B: A Unique Extragalactic Transient

Andrew J. Levan¹ , Antonio Martin-Carrillo² , Tanmoy Laskar³ , Rob A. J. Eyles-Ferris⁴ , Albert Sneppen^{5,6} ,
Maria Edvige Rivasio^{1,7} , Jillian C. Rastinejad⁸ , Joe S. Bright⁹ , Francesco Carotenuto¹⁰ , Ashley A. Chrimes^{1,11} ,
Gregory Corcoran² , Benjamin P. Gompertz¹² , Peter G. Jonker¹ , Gavin P. Lamb¹³ , Daniele B. Malesani^{5,6} ,
Andrea Saccardi¹⁴ , Javier Sánchez-Sierras¹ , Benjamin Schneider¹⁵ , Steve Schulze¹⁶ , Nial R. Tanvir⁴ ,
Susanna D. Vergani¹⁷ , Darach Watson^{5,6} , Jie An^{18,19} , Franz E. Bauer²⁰ , Sergio Campana⁷ , Laura Cotter² ,
Joyce N. D. van Dalen¹ , Valerio D'Elia²¹ , Massimiliano De Pasquale²² , Antonio de Ugarte Postigo¹⁵ , Dimple¹² ,
Dieter H. Hartmann²³ , Jens Hjorth²⁴ , Luca Izzo^{24,25} , Páll Jakobsson²⁶ , Amit Kumar²⁷ , Andrea Melandri¹⁰ ,
Paul O'Brien⁴ , Silvia Piranomonte¹⁰ , Giovanna Pugliese²⁸ , Jonathan Quirola-Vásquez¹ , Rhaana Starling⁴ ,
Gianpiero Tagliaferri⁷ , Dong Xu¹⁸ , and Makenzie E. Wortley¹² 

¹ Department of Astrophysics/IMAPP, Radboud University, P.O. Box 9010, 6500 GL Nijmegen, The Netherlands; a.levan@astro.ru.nl

² School of Physics and Centre for Space Research, University College Dublin, Belfield, Dublin 4, Ireland; antonio.martin-carrillo@ucd.ie

³Department of Physics & Astronomy, University of Utah, Salt Lake City, UT 84112, USA

⁴ School of Physics and Astronomy, University of Leicester, Leicester, LE1 7RH, UK

⁵ Niels Bohr Institute, University of Copenhagen, Jagtvej 155, 2200, Copenhagen N, Denmark

⁶The Cosmic Dawn Centre (DAWN), Denmark

⁷ INAF-Osservatorio Astronomico di Brera, Via Bianchi 46, I-23807, Merate (LC), Italy

⁸ Center for Interdisciplinary Exploration and Research in Astrophysics (CIERA) and Department of Physics and Astronomy, Northwestern University, Evanston, IL 60208, USA

⁹ Astrophysics, Department of Physics, University of Oxford, Keble Road, Oxford, OX1 3RH, UK

¹⁰ INAF-Osservatorio Astronomico di Roma, Via Frascati 33, I-00078, Monte Porzio Catone (RM), Italy

¹¹ European Space Agency (ESA), European Space Research and Technology Centre (ESTEC), Keplerlaan 1, 2201 AZ Noordwijk, The Netherlands

¹² School of Physics and Astronomy and Institute for Gravitational Wave Astronomy, University of Birmingham, Birmingham, B15 2TT, UK

¹³ Astrophysics Research Institute, Liverpool John Moores University, IC 2 Liverpool Science Park, 146 Brownlow Hill, Liverpool, L3 5RF, UK

¹⁴ Université Paris-Saclay, Université Paris Cité, CEA, CNRS, AIM, 91191, Gif-sur-Yvette, France

¹⁵ Aix Marseille Univ., CNRS, CNES, LAM, Marseille, France

¹⁶ Center for Interdisciplinary Exploration and Research in Astrophysics (CIERA), Northwestern University, 1800 Sherman Ave., Evanston, IL 60201, USA

¹⁷ LUX, Observatoire de Paris, Université PSL, CNRS, Sorbonne Université, Meudon, 92190, France

¹⁸ National Astronomical Observatories, Chinese Academy of Sciences, Beijing 100012, People's Republic of China

¹⁹ School of Astronomy and Space Science, University of Chinese Academy of Sciences, Chinese Academy of Sciences, Beijing 100049, People's Republic of China

²⁰ Instituto de Alta Investigación, Universidad de Tarapacá, Casilla 7D, Arica, Chile

²¹ Space Science Data Center (SSDC)—Agenzia Spaziale Italiana (ASI), Via del Politecnico snc, I-00133 Roma, Italy

²² MIFT Department, University of Messina, Via F. S. D'Alcontres 31, 98166, Messina, Italy

²³ Department of Physics and Astronomy, Clemson University, Clemson, SC 29634, USA

²⁴ DARK, Niels Bohr Institute, University of Copenhagen, Jagtvej 155A, 2200 Copenhagen, Denmark

²⁵ INAF, Osservatorio Astronomico di Capodimonte, Salita Moiarriello 16, I-80121 Naples, Italy

²⁶ Centre for Astrophysics and Cosmology, Science Institute, University of Iceland, Dunhagi 5, 107 Reykjavik, Iceland

²⁷ Department of Physics, Royal Holloway, University of London, Egham, TW20 0EX, UK


²⁸ Anton Pannekoek Institute of Astronomy, University of Amsterdam, P.O. Box 94249, 1090 GE Amsterdam, The Netherlands

Received 2025 July 18; revised 2025 August 6; accepted 2025 August 6; published 2025 August 29

Abstract

γ -ray bursts (GRBs) are singular outbursts of high-energy radiation with durations typically lasting from milliseconds to minutes and, in extreme cases, a few hours. They are attributed to the catastrophic outcomes of stellar-scale events and, as such, are not expected to recur. Here, we present observations of the exceptional GRB 250702B (formerly GRB 250702BDE) which triggered the Fermi GRB monitor on three occasions over several hours, and which was detected in soft X-rays by the Einstein Probe several hours before the γ -ray triggers (EP 250702a). We present the discovery of an extremely red infrared counterpart of the event with the Very Large Telescope, as well as radio observations from MeerKAT. Hubble Space Telescope observations pinpoint the source to a nonnuclear location in a host galaxy with complex morphology, implying GRB 250702B is an extragalactic event. The multiwavelength counterpart is well described with standard afterglow models at a relatively low redshift $z \sim 0.3$, but the prompt emission does not readily fit within the expectations for either collapsar or merger-driven GRBs. Indeed, a striking feature of the multiple prompt outbursts is that the third occurs at an integer multiple of the interval between the first two. Although not conclusive, this could be indicative of periodicity in the progenitor system. We discuss several possible scenarios to explain the exceptional properties of the burst, which suggest that either a very unusual collapsar or the tidal disruption of a white dwarf by an intermediate-mass black hole are plausible explanations for this unprecedented GRB.



 Original content from this work may be used under the terms of the [Creative Commons Attribution 4.0 licence](https://creativecommons.org/licenses/by/4.0/). Any further distribution of this work must maintain attribution to the author(s) and the title of the work, journal citation and DOI.

Unified Astronomy Thesaurus concepts: Gamma-ray bursts (629); Supernovae (1668); Core-collapse supernovae (304); X-ray transient sources (1852); Tidal disruption (1696)

1. Introduction

γ -ray bursts (GRBs) are brief flashes of high-energy radiation (peaking at $\sim 1\text{--}1000$ keV) with typical durations spanning from a fraction of a second (short GRBs), to minutes (long GRBs) (C. Kouveliotou et al. 1993), with only a tiny minority having durations up to a few hours (so-called ultralong GRBs; A. J. Levan et al. 2014). A key feature of GRBs is that they are singular, nonrepeating events that represent the final moments of stars, either via the collapse of a stellar core (e.g., J. Hjorth et al. 2003; K. Z. Stanek et al. 2003) or the merger of two compact objects (e.g., E. Berger et al. 2013; N. R. Tanvir et al. 2013; B. P. Abbott et al. 2017).

Although there is a great deal of diversity in individual GRB light-curve shapes, bursts at the extremes in duration or variability are rare and represent novel opportunities to search for GRB progenitors outside the accepted paradigm. For example, a subpopulation of the very shortest bursts arises from repeating sources—flares from magnetars, either within the Milky Way, or beyond (K. Hurley et al. 2005; E. Burns et al. 2021; S. Mereghetti et al. 2024; A. C. Trigg et al. 2025). In several instances, γ -ray emission has been indicative of relativistic outflows from a tidal disruption event (TDE; J. S. Bloom et al. 2011; D. N. Burrows et al. 2011; A. J. Levan et al. 2011; S. B. Cenko et al. 2012; G. C. Brown et al. 2015). However, in the case of TDEs, the related γ -ray light curves do not resemble GRBs, being longer-lived, but much less “bursty.”²⁹ Strikingly, although only a handful of GRB progenitors have been identified observationally, there are a large number of plausible routes that could lead to γ -ray emission, including events of significant astrophysical importance such as accretion-induced collapse (K. Nomoto & Y. Kondo 1991), disruptions of a white dwarf (WD) by an intermediate-mass black hole (IMBH, $\sim 10^3\text{--}10^5 M_\odot$; J. A. Irwin et al. 2010), micro-TDEs (H. B. Perets et al. 2016), other stellar mergers (C. L. Fryer et al. 1999; S. E. de Mink et al. 2014), or even explosions within common envelopes (C. L. Fryer et al. 1999; S. L. Schröder et al. 2020). Cases of rare GRBs therefore provide a novel route to identify some of the rarest but most astrophysically important events in nature.

Here, we present observations of a recently discovered series of GRB triggers (initially named GRBs 250702D, 250702B, and 250702E) which are unique in both their temporal and spatial coincidence and in their multiwavelength properties. We explore several progenitor scenarios for this series of GRB triggers and assess their viability. Throughout this work, we report all magnitudes in the AB system and assume a Λ CDM cosmology world model with $\Omega_M = 0.315$, $\Omega_\Lambda = 0.685$, and $H_0 = 67.4 \text{ km s}^{-1} \text{ Mpc}^{-1}$ (Planck Collaboration et al. 2020).

2. Observations

2.1. γ -Ray Detections

GRBs 250702D, 250702B, and 250702E (hereafter referred to as GRB 250702B)³⁰ were first discovered as a series of discrete triggers by the Fermi Gamma-Ray Burst Monitor (GBM; E. Neights et al. 2025a) on July 2 at 13:09:02, 13:56:06, and 16:21:33 UT, respectively.³¹ Throughout this work, δt refers to the time since the trigger time (T_0) of GRB 250702D. We note that the GRB 250702E trigger displayed an initial peak at $\delta t \sim 11,310$ s, which is 4 minutes prior to its GBM trigger time (E. Neights et al. 2025a) and which we use here when discussing timing. A fourth trigger (GRB 250702C) during this period was determined to be unrelated to GRB 250702B due to its position on the sky (E. Neights et al. 2025b). Konus-Wind also detected coincident hard X-ray (20–1250 keV, observer frame) emission spanning this period (D. Frederiks et al. 2025). Coincident prompt γ -ray to hard X-ray emission was also detected by Swift-BAT GUANO (A. Tohuvavohu et al. 2020; J. DeLaunay et al. 2025), MAXI/GSC (Y. Kawakubo et al. 2025), GECAM-B (C.-W. Wang et al. 2025), and the Space Variable Objects Monitor Gamma-ray Monitor (SVOM/GRM Team et al. 2025). We extract the Fermi/GBM γ -ray light curve of all three GRB triggers in the 8 keV–900 keV energy range from the daily data³² using the GBM Data Tools³³ and present it in Figure 1.

2.2. X-Ray Observations

The Einstein Probe (EP) Wide Field X-ray Telescope (WXT; H. Q. Cheng et al. 2025) detected an associated X-ray transient (EP 250702a) beginning on July 2 at 02:53:44 UT, 10.26 hr prior to the GBM triggers (H. Q. Cheng et al. 2025). Stacking of WXT observations revealed that X-ray emission from EP 250702a was already detectable on 2025 July 1. Observations by Swift-XRT beginning at $\delta t = 0.517$ day detected a bright, highly variable counterpart and provided the best X-ray position of R.A. (J2000) = $18^{\text{h}} 58^{\text{m}} 45^{\text{s}}.61$, decl. (J2000) = $-07^{\circ} 52' 26''.9$ (J. A. Kennea et al. 2025) with a $2''$ uncertainty.³⁴ Additional follow-up observations with NuSTAR were obtained starting at $\delta t = 1.317$ days and clearly detect a variable X-ray counterpart at 3–79 keV (B. O'Connor et al. 2025).

2.3. Optical and Near-Infrared Observations

We initiated optical and near-infrared (near-IR) observations of GRB 250702B with HAWK-I on the Very Large Telescope (VLT; program ID 114.27PZ, PIs: Malesani,

²⁹ The γ -ray-discovered events were located by searching for γ -ray triggers in reconstructed images rather than via the typical rate triggers.

³⁰ Due to the multiple GRB naming, this event was initially misnamed in GCNs as GRB 250702BDE. However, since these triggers came from the same source, we adopt the usual GRB naming convention of just one letter; in this case, the one from the first trigger announced.

³¹ Note that the alphabetical trigger names do not follow chronological order.

³² <https://heasarc.gsfc.nasa.gov/W3Browse/fermi/fermigdays.html>

³³ <https://fermi.gsfc.nasa.gov/ssc/data/analysis/gbm>

³⁴ The Swift/XRT data are automatically processed as described in P. A. Evans et al. (2007, 2009), and can be found at <https://www.swift.ac.uk/LSXPS/transients/9377>.

Table 1
Log of Optical/Near-IR Observations

Date	δt (days)	Telescope/Instrument	Filter	Magnitude	Magnitude (Host Sub)	References
2025-07-03 07:03:03	0.746	VLT/HAWK-I	<i>H</i>	20.78 ± 0.05	...	This work
2025-07-03 07:39:40	0.771	VLT/HAWK-I	<i>K</i>	19.36 ± 0.02	19.41 ± 0.02	This work
2025-07-03 17:26:10	1.179	WFST	<i>r</i>	>22.2	...	Y.-L. Hua et al. (2025)
2025-07-03 21:52:47	1.364	FTW/3KK	<i>r</i>	>23.6	...	M. Busmann et al. (2025)
2025-07-03 21:52:47	1.364	FTW/3KK	<i>i</i>	>22.7	...	M. Busmann et al. (2025)
2025-07-03 21:52:47	1.364	FTW/3KK	<i>J</i>	>21.7	...	M. Busmann et al. (2025)
2025-07-03 22:50:00	1.403	NOT/StanCAM	<i>i</i>	>24.9	...	This work
2025-07-03 23:45:36	1.442	CAHA2.2/CAFOS	<i>z</i>	>21.4	...	I. Pérez-García et al. (2025)
2025-07-04 03:20:59	1.591	VLT/HAWK-I	<i>K</i>	20.85 ± 0.03	21.05 ± 0.04	This work
2025-07-04 03:36:09	1.602	VLT/HAWK-I	<i>H</i>	22.39 ± 0.06	...	This work
2025-07-05 01:44:52	2.525	GTC/HiPERCAM	<i>g</i>	>23.6	...	This work
2025-07-05 01:44:52	2.525	GTC/HiPERCAM	<i>r</i>	>23.0	...	This work
2025-07-05 01:44:52	2.525	GTC/HiPERCAM	<i>i</i>	>22.6	...	This work
2025-07-05 01:44:52	2.525	GTC/HiPERCAM	<i>z</i>	>22.3	...	This work
2025-07-05 03:07:37	2.582	VLT/HAWK-I	<i>K</i>	21.49 ± 0.05	21.88 ± 0.08	This work
2025-07-05 10:14:00	2.878	Keck/MOSFIRE	<i>K</i>	21.7 ± 0.1	...	K. K. Das et al. (2025)
2025-07-05 10:14:00	2.878	Keck/MOSFIRE	<i>H</i>	>22.4	...	K. K. Das et al. (2025)
2025-07-05 10:14:00	2.878	Keck/MOSFIRE	<i>J</i>	>22.8	...	K. K. Das et al. (2025)
2025-07-06 02:16:22	3.547	GTC/EMIR	<i>Ks</i>	>21.5	...	This work
2025-07-08 02:43:27	5.567	GTC/EMIR	<i>Ks</i>	>22.0	...	This work
2025-07-08 06:50:09	5.737	VLT/HAWK-I	<i>K</i>	22.53 ± 0.06	24.17 ± 0.40	This work
2025-07-15 01:40:27	12.52	VLT/HAWK-I	<i>K</i>	22.82 ± 0.08	...	This work
2025-07-15 02:39:23	12.52	HST	F160W	24.80 ± 0.30	...	This work

Note. The time is given relative to the initial GBM trigger on GRB 250702D. Magnitudes were calibrated against UKIDSS nearby reference stars in Vega and then converted to AB by applying offsets of 1.900 (*K* band) and 1.379 (*H* band) (P. C. Hewett et al. 2006). Magnitudes are not corrected for Galactic extinction of $A_H = 0.158$, $A_K = 0.093$ (E. F. Schlafly & D. P. Finkbeiner 2011).

Tanvir, Vergani) starting on 2025 July 3 at 07:03:03 UT ($\delta t = 0.746$ day). We process all VLT observations using the ESO REFLEX packages, astrometrically align the HAWK-I observations to the Gaia reference frame, and perform photometric calibration with the UKIDSS Galactic Plane Survey (P. W. Lucas et al. 2008). We present a log of the HAWK-I observations in Table 1.

In our first epoch of HAWK-I imaging, we clearly detect a new source in both *H* and *K* bands within the Swift-XRT localization at R.A. (J2000) = $18^{\text{h}} 58^{\text{m}} 45^{\text{s}}.57$, decl. (J2000) = $-07^{\circ} 52' 26''.2$, with an uncertainty of $\sim 0''.1$ in each coordinate (Figure 2). We perform photometry on the source using small ($0''.5$) apertures, giving $K = 19.36 \pm 0.02$ mag, substantially brighter than the limiting magnitudes of archival VISTA observations of the field. We thus identify the source as the infrared counterpart of GRB 250702B (A. Martin-Carrillo et al. 2025). Notably, in our first epoch of imaging, the source shows an extremely red color of $H - K(\text{AB}) = 1.42 \pm 0.06$ mag (A. J. Levan et al. 2025b), which is 1.37 mag when considering the Milky Way extinction of $A_V = 0.847$ mag in the direction of the near-IR counterpart (E. F. Schlafly & D. P. Finkbeiner 2011), corresponding to an extremely steep spectral index of $\beta \approx -4$ (with $F_\nu \propto t^{\alpha} \nu^{\beta}$). In addition to the transient point source, our observations reveal potential underlying extension in the east–west direction, consistent with an underlying host galaxy (Figure 2). In later epochs of HAWK-I imaging, we continue to use narrow ($0''.5$) apertures to minimize host contamination, which increases in later epochs, in the photometry. We therefore also provide magnitudes from subtraction of the final HAWK-I epoch at $\delta(t) \sim 12.5$ days, although we note that there is still likely transient light in the

template epoch and the resulting magnitudes may be underestimated.

Following the HAWK-I near-IR detection, we obtained 4×600 s spectroscopy of the counterpart starting on 2025 July 4 at 03:26:53 UT ($\delta t = 1.60$ days) with the VLT X-shooter spectrograph (J. Vernet et al. 2011), covering 3000–24000 Å. We oriented the slit with a position angle of 90° to cover both the counterpart and the potential host galaxy, and employed the ABBA nod-on-slit mode. We reduce each individual exposure of the near-IR arm using the STARE mode reduction in the ESO REFLEX packages (a nodding reduction was not possible because of the presence of other objects in the slit). We subtract sky features and individually flux-calibrate each spectrum before combining into a final science spectrum (J. Selsing et al. 2019). The resulting 2D spectra show only a very faint trace across the *H* and *K* bands, highlighting the very red color of the transient (Figure 3), and the low signal-to-noise ratio of the data does not enable any useful constraints on the redshift of either the counterpart or the putative host galaxy.

We furthermore initiated a request for Directors Discretionary Time (DDT) observations with the Hubble Space Telescope (HST; program 17988, PI: Levan), and obtained a single orbit of observations with the F160W filter. We downloaded the flat-fielded, dark-subtracted, and image from the MAST archive, and redrizzled the individual exposures to a final pixel scale of $0''.07$. We detect both the near-IR counterpart as well as the underlying galaxy in the F160W image (Figure 2). The magnitude of the transient is highly uncertain because of contamination by galaxy light. Using a narrow aperture and on-galaxy background, we obtain

F160W = 24.8 ± 0.3 mag, but note that the uncertainty is likely underestimated due to systematics. We measure an offset between the point source and the galaxy centroid of $0''.7$.³⁵

We also obtained observations with the Gran Telescopio Canarias (GTC) using both the IR imager (EMIR) and the simultaneous multiband optical imager (HiPERCAM), as well as with the Nordic Optical Telescope (NOT), in multiple bands. We reduce observations using standard instrument pipelines. We do not recover the counterpart in any images, and report upper limits in Table 1. In addition to observations with our programs, we collect optical and near-IR data from the GCNs and summarize them in Table 1.

2.4. Radio Observations

We observed GRB 250702B with the MeerKAT radio telescope (F. Camilo et al. 2018; J. Jonas 2018) under program SCI-20241101-FC-01 (PI: Carotenuto) beginning on 2025 July 4 at 17:37:32 UT ($\delta t = 2.208$ days) at the S band (S4; central frequency 3.06 GHz and 875 MHz bandwidth), followed by a second observation on 2025 July 8 at 18:43:45 UT ($\delta t = 6.236$ days) at the L band (central frequency 1.28 GHz and 856 MHz bandwidth). We utilize PKS J1939–6342 as bandpass and flux density calibrator and J1822–096 and J1908–201 as complex gain calibrators at 3.06 and 1.28 GHz, respectively, obtaining a total on-source time of 42 minutes in each band. We reduce the data with the OXKAT pipeline (I. Heywood 2020), which performs standard flagging, calibration, and imaging using tricolour (B. V. Hugo et al. 2025), CASA (CASA Team et al. 2022), and WSCLEAN (A. R. Offringa et al. 2014), respectively. For imaging, we adopt a Briggs weighting scheme with a -0.3 robustness parameter for both frequencies, which yielded a beam of $10''.9 \times 2''.7$ and rms noise of $9 \mu\text{Jy beam}^{-1}$ at 3.06 GHz, and $8''.1 \times 6''.4$ and $13 \mu\text{Jy beam}^{-1}$ at 1.28 GHz. We clearly detect the radio counterpart of GRB 250702B at the position of the optical counterpart at both frequencies (first reported in A. J. Bright et al. 2025). We fit for a point source in the image plane and report our results in Table 2. We additionally compile publicly reported millimeter and radio observations from MeerKAT, the Atacama Large Millimeter Array (ALMA; K. D. Alexander et al. 2025), the James Clark Maxwell Telescope (JCMT; A. J. Tetarenko et al. 2025), the Allen Telescope Array (Allen TA; A. I. Sfaradi et al. 2025b), and the Karl G. Jansky Very Large Array (VLA; A. I. Sfaradi et al. 2025b) in Table 2.

3. Host Galaxy

The combination of the offset and measured K -band magnitude of the underlying galaxy enables us to calculate the probability of chance alignment (P_{cc}). Following the methodology of J. S. Bloom et al. (2002), but with number counts updated and appropriate for our K -band observations (R. A. Windhorst et al. 2023), we find $P_{cc} \lesssim 0.1\%$. We therefore conclude that, despite a location close to the Galactic plane ($b = -5.2^\circ$), the underlying galaxy is the host and that GRB 250702B is an extragalactic event.

The galaxy is clearly resolved in HST images and visible as an extension in the HAWK-I images with good seeing. As the source is relatively extended and shows low-surface-brightness regions that overlap with foreground objects, accurate total photometry is particularly complex. Using an elliptical aperture of semimajor/minor axis $1''.75/0''.65$, we measure magnitudes of $K(\text{AB}) = 20.78 \pm 0.05$ and F160W (AB) = 21.55 ± 0.09 , and a half-light radius of approximately $0''.8$. Alternatively, using GALFIT (C. Y. Peng et al. 2010) and two Sérsic functions, the best-fit model returns a mean half-light radius of $0''.9 \pm 0''.1$, fully consistent with the elliptical aperture measurement.

In the HST images the galaxy appears split into two separated regions. This may be due to some form of ongoing interaction, but is also reminiscent of strong dust lanes observed frequently from edge-on disk-like galaxies. The lane appears to extend across the nucleus of the galaxy in the direction of the near-IR counterpart; thus, if the transient lies within (or behind) the dust lane, dust extinction would provide a natural explanation for the observed extreme redness (Section 2.3).

No spectroscopic redshift for the galaxy is available at the time of writing. Existing detections, which are limited to F160W/ H and K bands, are insufficient to derive a photometric redshift. However, the galaxy appears relatively large and well resolved, revealing substructure at the resolution of the HST observations, and enabling some constraints on its redshift. These are discussed in more detail in Appendix B, but briefly. At low redshift ($0.1 < z < 0.5$), the host is consistent with both the galaxy size distribution (K. Ormerod et al. 2024) and the sizes and absolute magnitudes of known GRB hosts (e.g., J. D. Lyman et al. 2017; B. Schneider et al. 2022). At higher redshift, it would be an unusually large and luminous galaxy. Such galaxies are rare, although not unheard of. Hence, we cannot robustly constrain the redshift, aside from noting that it would have unprecedentedly high luminosity if beyond $z \sim 2-3$. However, the galaxy properties do favor a lower- z scenario with $z < 1$ (and most likely at $z < 0.5$), in keeping with constraints from the afterglow and absorption properties (see Section 5).

4. A Repeating, Extragalactic GRB

Numerous properties of GRB 250702B are unique or extreme when compared to those typically seen in GRBs. The first reported high-energy detections predate the final GBM trigger by a day (Section 2.2). Whereas most GRBs are brightest in the γ -rays within seconds to minutes of the trigger time, there were no γ -ray triggers from GRB 250702B prior to T_0 , despite the earlier detections by the EP (H. Q. Cheng et al. 2025). Further, the most energetic outburst was at the time of the final trigger (GRB 250702E; E. Neights et al. 2025b), with the fluence of the three bursts reported as 1.04×10^{-5} , 1.24×10^{-5} , and $2.74 \times 10^{-5} \text{ erg cm}^{-2}$. Hence, both in timescale and light-curve morphology, GRB 250702B seems to be substantially different from the bulk of the GRB population.

The timing of the three triggers further exhibits interesting patterns. Whereas the time difference between the first and second GRB triggers is 2825 s, the third trigger (GRB 250702E) begins at a near-integer time step from this, corresponding to close to 4 times the 2825s interval (i.e., $(4 \times 2825) + 4$ s later). This could be interpreted as a period of repetition in the GRB triggers with potential implications for

³⁵ We note that the galaxy centroid is not well defined, since it is divided into two visible regions in the HST imaging (Figure 2). However, the offset from either to the GRB position is comparable.

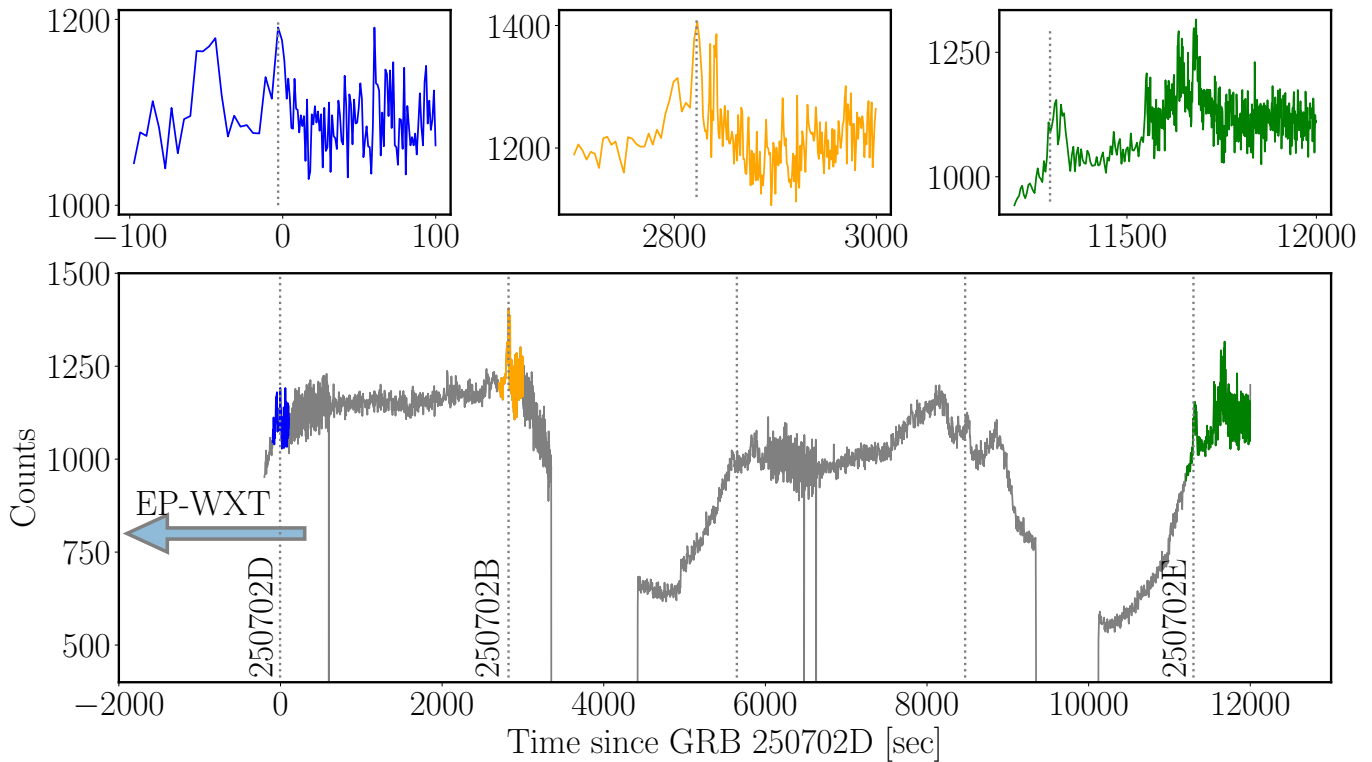


Figure 1. The Fermi-GBM (8 keV –900 keV energy range; observer frame) count-rate light curve spanning from -2×10^3 to 1.2×10^4 s after the GRB 250702D trigger (main panel, gray lines; with data from each burst highlighted in color), along with zoom ins around the time of the individual triggers (upper row). EP-WXT observations revealed an X-ray counterpart a day earlier (blue arrow; H. Q. Cheng et al. 2025), indicating transient high-energy emission preceding the GBM trigger. The dashed vertical lines indicate periods of 2825 s (the measured gap between GRB 250702D and GRB 250702B).

the progenitor. If so, these three triggers correspond to the first, second, and fifth “beat” of the period. No γ -ray triggers have been reported coincident with the third and fourth beat. Although plausible subthreshold structure is visible within the γ -ray light curves (Figure 1), the complex background precludes any robust statements about the presence of possible emission at these times. We consider the possible physical implications of this potential periodicity in Section 6.1.

Although there is no precise redshift available for GRB 250702B, the presence of a relatively bright and extended host galaxy suggests the redshift is low ($z < 1$; Section 3 and Appendix B), and our afterglow modeling (Section 5) favors a $z \sim 0.3$ origin. Using these constraints, we next consider how the energetics of the burst would appear at redshifts in the interval $0.1 < z < 1$. Unsurprisingly $E_{\gamma, \text{iso}}$ varies dramatically across this broad redshift range. Using the integrated Konus-Wind flux for GRB 250702B, the E_{iso} ranges from 1.4×10^{52} erg ($z = 0.1$) to 1.6×10^{54} ($z = 1.0$), which are both consistent with the bulk GRB population (e.g., A. Tsvetkova et al. 2017). However, attempts to fit typical GRB-like Band functions (D. Band et al. 1993) to the spectra yield high E_p of several hundred keV (E. Neights et al. 2025b). Notably, across the redshift range considered here, this lies substantially in excess of the E_p – E_{iso} relations (e.g., L. Amati 2006). The same is true, and indeed becomes more acute, if considering each individual trigger (“D,” “B,” “E”) separately.

5. Afterglow Properties

While the prompt emission seems unusual, the afterglow is more readily comparable to those of the typical GRB

population. Across the range $0.1 < z < 1$, the X-ray and radio luminosity is consistent with GRB afterglows (e.g., Figure 4; P. Chandra & D. A. Frail 2012; A. de Ugarte Postigo et al. 2012). Though the near-IR emission is unusually red, its absolute magnitude is also in keeping with those seen for other GRB afterglows (e.g., D. A. Kann et al. 2024).

We now consider whether these observations are consistent within the framework of the standard GRB fireball model, where synchrotron afterglow emission arises from shocks produced in the interaction of a collimated, relativistic jet with the ambient medium (see Figure 5, left panel). Such a model is clearly applicable in a standard GRB progenitor paradigm, but its validity with alternative central engines is less obvious and may depend on the details of the engine. The details of our modeling are discussed in Appendix A. We keep the redshift as a free parameter in the range $0.1 < z < 12$, and find that forward shock (FS) emission fits the optical and X-ray observations well, provided $z \lesssim 0.3$ and $A_V \gtrsim 10$ mag. Higher-redshift models, while requiring lower A_V (due to the near-IR observations probing bluer rest-frame filters), push³⁶ the outflow’s isotropic-equivalent energy ($E_{K, \text{iso}}$) beyond our maximum allowed value of 5×10^{54} erg (appropriate for GRBs and jetted TDEs; e.g., S. B. Cenko et al. 2011; P. Beniamini et al. 2023) and are disfavored (see Figure 6 in Appendix A). The observed steep X-ray and optical light curves are further consistent with an early jet break ($t_{\text{jet}} \lesssim 0.5$ day). The radio observations in this framework require an additional component, e.g., a reverse shock

³⁶ This degeneracy maintains a high cooling frequency, $\nu_c \gtrsim \nu_X$, which is required for matching the dereddened near-IR colors and the near-IR to X-ray spectral index at higher z within our allowed constraint of $2 < p < 3$.

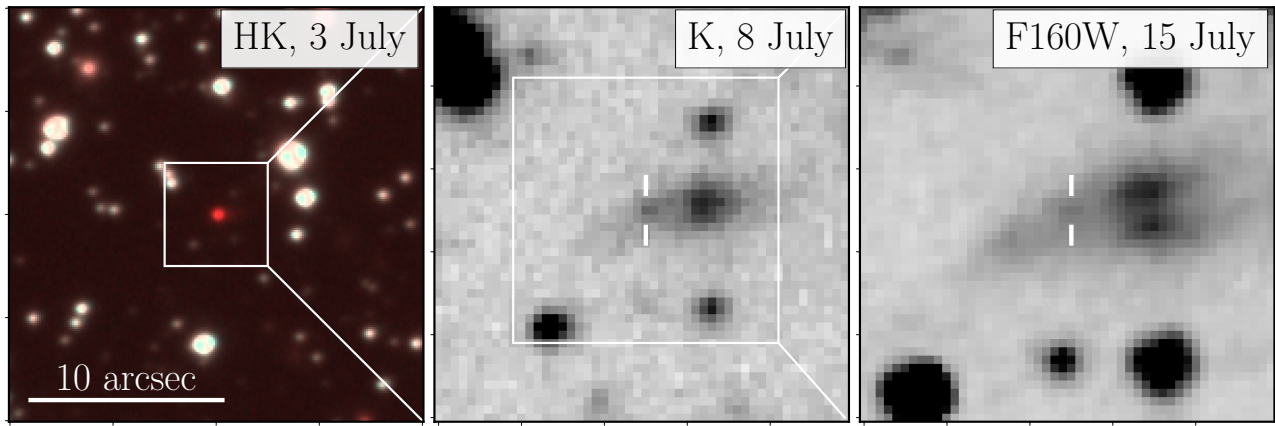


Figure 2. Left: discovery image of the counterpart of GRB 250702B obtained with the VLT/HAWK-I. The false-color composite is constructed from the H - and K -band observations and demonstrates the transient’s extremely red color. Middle: zoomed-in region (corresponding to the white box in the left panel) around GRB 250702B’s counterpart at $\delta t = 5.737$ days as observed with HAWK-I in excellent seeing conditions. The transient appears to be offset from a likely extended source. Right: HST imaging clearly resolves the extended source, revealing a complex, asymmetric morphology, as well as the possible presence of a strong dust lane through the disk of the galaxy.

(RS; Figure 5, right panel). In our modeling, we keep this component fixed (due to the paucity of radio data) and vary the FS parameters. Besides an extremely narrow opening angle ($\theta_{\text{jet}} \approx 0.4^\circ$, driven by the early jet break, high $E_{K,\text{iso}}$, and low density), the inferred parameters are consistent with those previously inferred for GRBs (e.g., T. Laskar et al. 2014). For our best-fit parameters, we infer a prompt efficiency of $\eta_\gamma \approx 10\%$ and an FS Lorentz factor of $\Gamma_{\text{FS}} \approx 40$ at the time of the first detection, $\delta t \approx 0.5$ day, also consistent with GRB afterglows (T. Laskar et al. 2014; G. Ghirlanda et al. 2018).

The high local host extinction is also consistent with the observed large X-ray absorption column, $N_{\text{Hx}} \approx (1.1 \pm 0.2) \times 10^{22} \text{ cm}^{-2}$ (corresponding to $N_{\text{Hx}} \approx (8.6 \pm 2.0) \times 10^{21} \text{ cm}^{-2}$ after subtracting the Galactic contribution; P. A. Evans et al. 2007, 2009). We can formalize this by computing a redshift using the correlation between X-ray and dust column (e.g.,

D. Watson 2011), $z = \left(\frac{2 \times 10^{21} \text{ cm}^{-2} \text{ mag}^{-1}}{N_{\text{Hx}}(z=0) / A_V(z)} \right)^{\frac{1}{2.4}} - 1$ (Appendix B).

Using our inferred host galaxy $A_V(z=0)$ posterior and additional statistical uncertainties (Appendix B), this gives a redshift of $z = 0.50 \pm 0.29$, consistent with the host properties (Section 3) and the afterglow modeling (Appendix A). One caveat here is that for classical GRBs this ratio is an order of magnitude larger (e.g., P. Schady et al. 2010), probably due to a large column density of ionized, dust-free gas close to the GRB site (D. Watson et al. 2013). Thus, if this was a classical GRB, then the redshift inferred above is a lower limit. This constraint provides further evidence the burst is not Galactic, because the metals providing the dust column would be detected in stronger X-ray absorption than is observed.

6. Progenitor Scenarios

The host association for GRB 250702B presented here rules out a Galactic origin for the transient (e.g., X-ray binaries, cataclysmic variables, novae, magnetars, etc.). However, the key question relating to GRB 250702B is the identity of its progenitor. As a series of long GRBs, does it arise from a stellar-scale core-collapse event, as is apparently the case for the ultralong GRBs (J. Greiner et al. 2015)? Alternatively, given its unprecedented nature, does it arise from a potentially previously unseen kind of object? The match of the available

observations to fireball models may suggest a collapsar origin, but other progenitors may produce observationally similar emission. Here, we consider several possible progenitor scenarios for GRB 250702B, and contrast these against available observations.

6.1. A Relativistic TDE

A known source class that can produce high-energy emission on \sim hours to days timescales is relativistic TDEs powered by super-Eddington accretion onto a massive black hole. Highly variable γ -ray light curves similar to GRB 250702B have previously been observed in relativistic TDEs, specifically Swift J1644+57 (e.g., D. N. Burrows et al. 2011; A. J. Levan et al. 2016; V. Mangano et al. 2016), which triggered Swift-BAT (via an image trigger) four times over 2 days with a comparable inter-trigger interval to GRB 250702B. The high γ -ray variability, hard-to-soft X-ray spectral evolution, and variable (but nonflaring) hard X-ray properties are all consistent with the early behavior of past relativistic TDEs (D. N. Burrows et al. 2011; S. B. Cenko et al. 2012; D. R. Pasham et al. 2015; V. Mangano et al. 2016). This similarity extends further with consistencies between the near-IR power-law decay and self-absorbed radio emission of GRB 250702B and these past events (A. J. Levan et al. 2016; E. Hammerstein et al. 2025). Underneath the short-term variability, the early X-ray light curve of relativistic TDEs typically follows a power-law decay, sometimes consistent with the canonical $t^{-5/3}$ decay in the fallback rate, \dot{m}_{fb} (M. J. Rees 1988). However, this can be steeper and consistent with the decay ($\alpha_X = -2.0 \pm 0.1$) we see in GRB 250702B due to factors we discuss below.

We consider three possible TDE scenarios for GRB 250702B that produce sufficiently super-Eddington accretion rates to drive a relativistic jet: (1) a main-sequence (MS) star disrupted by a supermassive black hole (SMBH, $\sim 10^5 - 10^7 M_\odot$), (2) a MS disrupted by an IMBH, and (3) a WD disrupted by an IMBH. Notably, each of these is observationally rare, with only four MS-SMBH TDE candidates (e.g., J. S. Bloom et al. 2011; D. N. Burrows et al. 2011; A. J. Levan et al. 2011; S. B. Cenko et al. 2012; G. C. Brown et al. 2015; I. Andreoni et al. 2022; D. R. Pasham et al. 2023) and even fewer IMBH TDE candidates (e.g., P. G. Jonker et al. 2013;

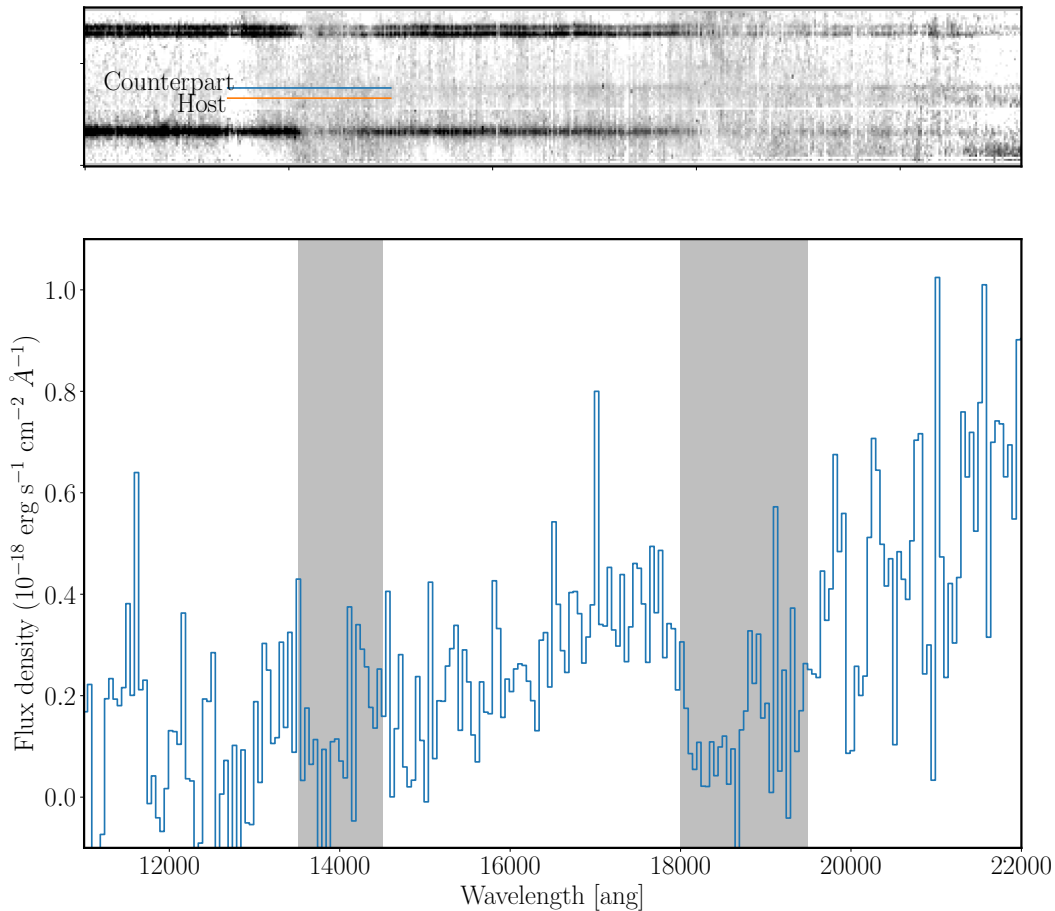


Figure 3. X-shooter spectroscopy in 2D (top) and 1D (bottom) of the counterpart of GRB 250702B obtained on 2025 July 4, rebinned in the 1D to 50 Å per bin. Signal is only recovered in the infrared arm (shown) at low signal to noise. The gray bands indicate regions of high telluric absorption that are not corrected for. The source shows brightening through the H and K regions of the spectrum consistent with photometry. Given the low signal to noise no significant absorption or emission features are visible in the counterpart spectrum. The slit was also oriented to cover the location of the host galaxy, but no redshift could be derived.

C. C. Jin et al. 2025), although the latter have also been considered for ultralong GRBs (e.g., A. J. Levan et al. 2014; M. MacLeod et al. 2016).

The nonnuclear location of GRB 250702B in the host galaxy (Figure 2) makes the first scenario unlikely but still feasible if, for example, the host is undergoing a merger. As this is difficult to assess at present, we disfavor but do not rule out this scenario.

Distinguishing between the second (MS-IMBH) and third (WD-IMBH) scenarios is harder, but may be possible if the periodicity between the triggers (Section 4) is associated with the orbital period of the disrupted star (i.e., the γ -ray flares correspond to mass transfer caused by partial disruptions). In this case, we can compare the required circular orbital radius, the innermost stable circular orbit for a range of black hole masses, and the Roche limits for $1 M_{\odot}$ MS and WD stars. This reveals that only WD-IMBH disruptions are consistent with the periodicity. The short-term (~ 100 s) variability observed in the light curve is also easier to achieve if associated with precession, as suggested for Swift J1644+57 (J. H. Krolik & T. Piran 2011). In the TDE scenario, we thus favor the WD-IMBH explanation; however, we note that the multiple bursts may also be driven by a jet or accretion timescale unrelated to an orbital period (e.g., precession). Indeed, an accreting WD scenario (A. King 2022) has also been considered for the class

of quasiperiodic eruptions (e.g., G. Miniutti et al. 2019), to which GRB 250702B could belong.

For a fiducial $10^4 M_{\odot}$ IMBH and $0.5 M_{\odot}$ WD, assuming the periastron radius is equal to the tidal radius, an eccentricity of order $e \sim 0.955$ is required. This could plausibly be achieved through Hills capture (J. G. Hills 1988) and would require an impact parameter of $\beta \sim 2$ for the original binary (M. Cufari et al. 2022a). The eccentricity inferred above can result in a steeper X-ray decline than the typical $t^{-5/3}$ decay rate (M. Cufari et al. 2022b). We test this using the “frozen-in” approximation³⁷ with the $10^4 M_{\odot}$ IMBH, $0.5 M_{\odot}$ WD, and $e = 0.955$ above. We fix the peak fallback time to the Fermi-GBM trigger time of GRB 250702E (E. Neights et al. 2025a) and, assuming an accretion efficiency of order 0.01 and $z \sim 0.14$ to match the observed luminosity of Swift J1644+57, find a reasonable match to the X-ray light curve.³⁸

Overall, if GRB 250702B is indeed a relativistic TDE, the data discussed here likely sit within the jet-dominated phase,

³⁷ We note that M. Cufari et al. (2022b) do find significant differences between this analytical approximation and numerical simulations but these dominate at more extreme eccentricities.

³⁸ While the jet physics involved are complex, if the jet luminosity is dominated by the accretion rate, the difference in slope could also be attributable to a full disruption ($\dot{m}_{\text{fb}} \propto t^{-5/3}$) in Swift J1644+57 and a partial disruption ($\dot{m}_{\text{fb}} \propto t^{-9/4}$) in other events including GRB 250702B (C. J. Nixon et al. 2021; T. Eftekhari et al. 2024).

Table 2
Log of Radio/Submillimeter Observations Presented in This Work or Publicly Available

Date	δT (days)	Telescope	Frequency (GHz)	Flux Density (mJy beam ⁻¹)	References
2025-07-04 07:37:01	1.769	Allen TA	5	<1.1	A. I. Sfaradi et al. (2025a)
2025-07-04 18:08:44	2.208	MeerKAT	3.06	0.12 ± 0.01	This work
2025-07-06 18:53:41	4.239	MeerKAT	1.28	0.1	P. Atri et al. (2025)
2025-07-08 18:43:45	6.236	MeerKAT	1.28	0.08 ± 0.01	This work
2025-07-08 05:59:11	5.701	VLA	10	0.49 ± 0.05	A. I. Sfaradi et al. (2025b)
2025-07-08 21:05:00	6.331	JCMT	350	<6.3	A. J. Tetarenko et al. (2025)
2025-07-09 02:09:03	6.542	ALMA	97.5	2	K. D. Alexander et al. (2025)

Note. The time is given relative to the initial GBM trigger on GRB 250702D.

which is seen to last of order months to years in other events (B. A. Zauderer et al. 2013; G. C. Brown et al. 2015; D. R. Pasham et al. 2015; T. Eftekhari & E. Berger 2017; T. Eftekhari et al. 2024).

A distinguishing signature of a relativistic TDE is the X-ray emission entering a steep decline as the accretion rate drops below the Eddington limit and the jet turns off (D. R. Pasham et al. 2015; A. J. Levan et al. 2016; T. Eftekhari et al. 2024). Based on the analytical WD-IMBH model described above, we estimate this will occur at ~ 40 days in the observer frame. We note that due to the degeneracy of the efficiency and redshift, the steep decline may occur \sim months to years later, particularly if the IMBH is less massive than assumed. The radio counterparts of relativistic TDEs continue to rise for hundreds to thousands of days, and may also show evidence for multiple components (B. A. Zauderer et al. 2013; D. R. Pasham et al. 2015; T. Eftekhari & E. Berger 2017; O. Teboul & B. D. Metzger 2023; L. Rhodes et al. 2025). In this case, multiple components could be expected in a similar fashion to Swift J1644+57 (e.g., O. Teboul & B. D. Metzger 2023), while the rise could be curtailed at relatively early times if the jet shuts off in line with our prediction. Long-term X-ray and radio monitoring is therefore crucial to evaluating this explanation.

6.2. GRB from an Atypical Stellar Core Collapse

The majority of long-duration GRBs appear to arise from the core collapse of massive stars (e.g., J. Hjorth et al. 2003; K. Z. Stanek et al. 2003), although a substantial minority now also seem to arise from compact object mergers (e.g., J. C. Rastinejad et al. 2022; E. Troja et al. 2022; J. Yang et al. 2022; A. J. Levan et al. 2024; Y.-H. Yang et al. 2024). Stellar core-collapse models for GRBs associate jet lifetimes (and hence prompt emission durations) with the freefall timescale, which are typically limited to a few seconds (S. E. Woosley et al. 2002). In principle, the duration of the GRB reflects the lifetime of the central engine *after* the jet has pierced the star (O. Bromberg et al. 2013). The time for the jet to traverse the star is a few seconds for a compact stripped progenitor, up to a few hours for the collapse of giant stars (A. J. Levan et al. 2014). In this scenario, the EP detection implying a prompt emission duration $\gtrsim 50$ ks remains a challenge. However, this timescale may be extended somewhat via a variety of routes including rapidly rotating progenitors (H. J. van Eerten 2014; P. C. Duffell & A. I. MacFadyen 2015), close binary progenitors (M. V. Barkov & S. S. Komissarov 2010), invoking magnetic support from the accretion disk (N. M. Lloyd-Ronning et al. 2016), tapping angular momentum from the black hole (M. H. P. M. van Putten 1999; C. L. Fryer et al. 2025), or via accretion disk

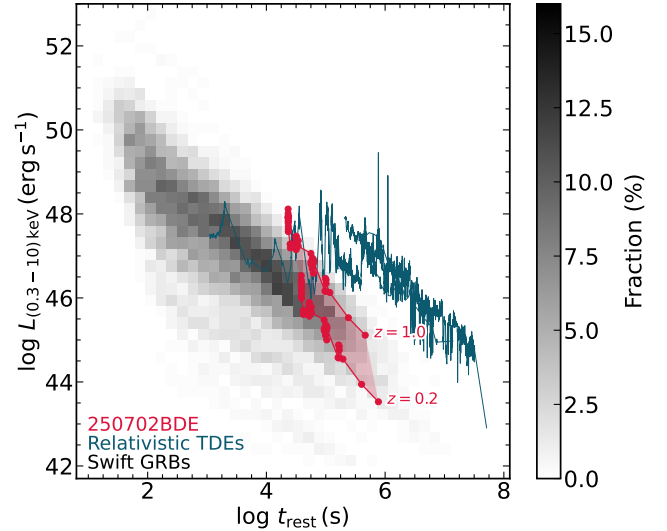


Figure 4. Comparison of the X-ray light curve of GRB 250702B with those of Swift GRBs (grayscale background) and relativistic TDE candidates, downloaded from the Swift Burst Analyser (P. A. Evans et al. 2007, 2009, 2010) and the Living Swift-XRT Point Source Catalogue (P. A. Evans et al. 2023) and processed as described in S. Schulze et al. (2014). At any reasonable redshift the luminosity of the event is comparable to those of GRBs, and GRB 250702B is clearly faster and less luminous than the relativistic TDE candidates. This would be consistent with a lower-mass black hole involved in a disruption, or with a more normal GRB interpretation.

instabilities (R. Perna et al. 2006). Alternatively, magnetars have also been widely discussed as a route to longer-lived emission in GRBs, including in ultralong events (e.g., B. D. Metzger et al. 2015), although magnetar engines have a maximal total energy of $\sim 10^{52}$ erg due to the limited energy stored in the spin of the magnetar. In the case of GRB 250702B, the combination of morphology (starting faint and getting brighter) and prompt energy correlations (away from the $E_p - E_{\text{iso}}$ relations) further challenge the interpretation of GRB 250702B as a core-collapse event.

Although several lines of evidence point away from a collapsar, it should also be noted that several others are entirely in keeping with a collapsar origin. These include the overall energetics, afterglow properties, and the location within the host galaxy. Although the afterglow is highly extinguished, there is strong precedent for this in the dark GRB population (A. Melandri et al. 2012; K. M. Svensson et al. 2012; D. A. Perley et al. 2013; G. Schroeder et al. 2022).

As a rare event it is also possible that unusual and rare circumstances are at play in GRB 250702B that do not impact the general GRB population, including GRBs originating at

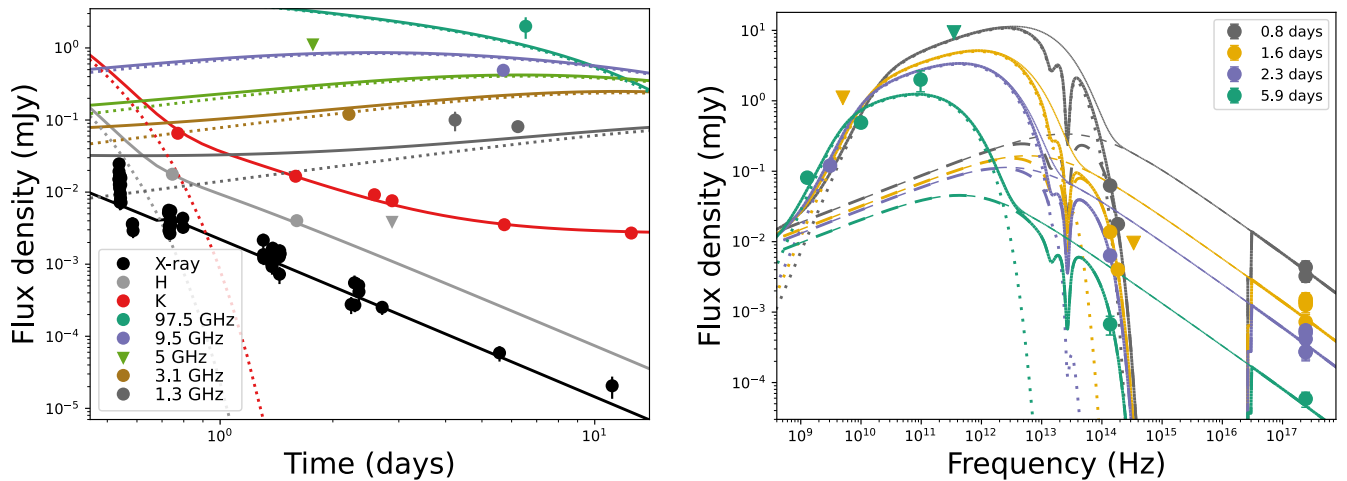


Figure 5. Light curves (left) and spectral energy distributions (right) for the afterglow of GRB 250702B spanning from ≈ 0.5 to 20 days at radio to X-ray wavelengths. The observations can be well explained by a standard synchrotron model comprising radiation (solid lines) from forward (dashed) and reverse (dotted) shocks at $z \approx 0.16$ and high host attenuation, $A_V \approx 12$ mag (see Section 5 for details and Appendix A for model parameters).

unusual phases of stellar evolution. This might include explosions within a common envelope (e.g., S. L. Schröder et al. 2020) that could create complex circumstellar media into which the jet propagates and the γ -rays are scattered, the collapse of particularly massive stars formed dynamically in extremely dense stellar clusters (e.g., S. F. Portegies Zwart et al. 2004), or even stellar collapse inside a very tight binary containing a second compact object in which complex fallback processes impact the resulting light curves (e.g., R. P. Church et al. 2012). Hence, while clearly exhibiting a set of prompt properties inconsistent with those of GRB-supernovae seen before, these do not automatically rule out a stellar collapse origin. Indeed, such origins have even been suggested for the population of events now generally interpreted as relativistic TDEs (E. Quataert & D. Kasen 2012).

For a moderately low redshift it may ultimately be possible to observe any associated supernova, although the extinction will require K -band observations where supernovae are unfortunately not especially bright. At $z \sim 0.3$, we might expect a supernova near-IR peak around $K \sim 22$ mag. Ground-based near-IR observations may be sensitive to supernovae even in cases where $A_K > 2$, and the James Webb Space Telescope (JWST) could probe to very high extinctions ($A_K > 10$). For comparison, our afterglow modeling indicates $A_K \sim 1.7$ mag, suggesting that a deep ground-based supernova search may yet be viable.

6.3. A GRB with Dust Echoes

The repeating nature of GRB 250702B shares some superficial similarities with GRB dust echo models (in which the prompt emission is Compton scattered by circumstellar material; e.g., C. D. Dermer et al. 1991; S. Klose 1998; P. Madau et al. 2000; J. A. Moran & D. E. Reichart 2005; K. Heng et al. 2007; L. Shao et al. 2008). The ~ 1 hr long timescale between peaks corresponds to an extremely compact physical scale of ~ 10 au for the scattering surfaces. In this interpretation, the distinct peaks require a specific configuration of the circumstellar medium, namely dense, thin shells (P. Madau et al. 2000). Although the event apparently occurred in a dusty environment, the spatial scale implied by these

timescales is small enough that dust destruction by the GRB radiation field should be significant (K. Heng et al. 2007), decreasing the opacity and reducing the luminosity of the echoes. This is in contrast with GRB 250702B, which has similar (or even increasing) peak count rates in each of the three triggers (Figure 1). On the other hand, the different distances associated with different parts of the scattering shells would naturally extend the prompt duration. Furthermore, the spectrum of the scattered prompt emission is expected to be significantly attenuated at energies above ~ 100 keV and to soften over time (C. D. Dermer et al. 1991; L. Shao & Z. G. Dai 2007). This is at odds with the high peak energy (and increasing spectral hardness) seen in the Fermi-GBM triggers.

6.4. A (Lensed) High- z GRB

The very red $H - K$ color could be explained by the presence of the $\text{Ly}\alpha$ break in the H band, placing the burst at $z \sim 12$. In this case, the foreground galaxy would either be a chance alignment, or more likely (see below) acting as a lens for the GRB. GRBs spawned from first-generation (Population III) stars may be both extremely energetic, $E_{\gamma, \text{iso}} \gtrsim 10^{55}$ erg, and long-lasting, $t_{\text{dur}} \gtrsim 10^3 \times (1 + z)$ s, because of their extended envelopes (Y. Suwa & K. Ioka 2011). At $z \sim 12$, the isotropic energy of the GRB would be $\sim 10^{56}$ erg, an extreme value,³⁹ but may still render the energetics consistent with the $E_p - E_{\text{iso}}$ relation (Section 4). Alternatively, the long duration of the event could be due to lensing, with the same burst repeating multiple times. The concept of repeating GRBs as lensed events stretches back to some of the first suggestions of extragalactic origin (e.g., B. Paczynski 1986), and a handful of claimed lensed GRBs have been suggested in the literature (see A. J. Levan et al. 2025a for a review).

However, while such a high- z event would be of extreme importance, our X-shooter spectroscopy shows the source to be red across the spectral window, without a strong break. Hence, a high- z event (lensed or not) would also need to be intrinsically red (and hence its afterglow even brighter

³⁹ Currently, the highest isotropic energy measured for a GRB is $\sim 2 \times 10^{55}$ erg for GRB 221009A (e.g., E. Burns et al. 2023; D. B. Malesani et al. 2023; J.-L. Atteia et al. 2025).

allowing for this extinction). Furthermore, although the signal-to-noise of the prompt emission is not high, the morphology of the burst light curves appears to be different, disfavoring the lensing origin.

7. Conclusion

We have presented new, multiwavelength observations of a superlative series of associated GRB triggers, GRB 250702B. Our observations reveal a rapidly fading, multiwavelength counterpart embedded in a galaxy with a complex and asymmetric morphology. We identify this galaxy as its host, and conclude that GRB 250702B is an extragalactic event. The relatively bright and extended host suggest the redshift is moderate ($z < 1$).

GRB 250702B is observationally unprecedented in its timescale, morphology, and the onset of X-ray photons prior to the initial GRB trigger (H. Q. Cheng et al. 2025). In addition, we find a striking, near-integer time step between the GRB outbursts, suggesting (although not proving) possible periodicity in the events.

We find that a standard afterglow FS and RS model can explain the multiwavelength light curves of the burst counterpart. The model favors high local host attenuation ($A_V \approx 11$ mag) and a low-redshift origin, leaving open several possible progenitor theories. We explore several models for this unusual event, including a relativistic TDE, a rare, nonstandard collapsar, a typical collapsar which produces GRB dust echoes, and a lensed, high-redshift event. We find that an atypical collapsar and a possibly repeating WD-IMBH TDE are most compatible with current available information.

Looking forward, high-resolution observations of GRB 250702B's local environment, continued X-ray and radio monitoring of its counterpart, and a deep near-IR supernova search are promising routes to further constrain its origins. Future detections of such events, especially those exhibiting periodicity, offer the chance to constrain their rates and decipher their origins, while continued wide-field high-energy γ -ray and X-ray monitoring capability remains essential for their prompt discovery and identification.

Acknowledgments

We would like to thank the anonymous referee for their timely and useful comments that have helped improving the quality of the Letter. Based on observations collected at the European Southern Observatory under ESO program(s) 114.27PZ. This work is based on observations made with the NASA/ESA Hubble Space Telescope. The data were obtained from the Mikulski Archive for Space Telescopes at the Space Telescope Science Institute, which is operated by the Association of Universities for Research in Astronomy, Inc., under NASA contract NAS 5-03127 for JWST. These observations are associated with program 17988.

Based on observations made with the Gran Telescopio Canarias (GTC), installed at the Spanish Observatorio del Roque de los Muchachos of the Instituto de Astrofísica de Canarias, on the island of La Palma under programmes GTC1-24ITP (PI: Peter Gustaaf Jonker) & GTCMULTIPLE3C-25A (PI: Daniel Mata Sanchez).

Based on observations made with the Nordic Optical Telescope, owned in collaboration by the University of Turku and Aarhus University, and operated jointly by Aarhus

University, the University of Turku and the University of Oslo, representing Denmark, Finland and Norway, the University of Iceland and Stockholm University at the Observatorio del Roque de los Muchachos, La Palma, Spain, of the Instituto de Astrofísica de Canarias. The NOT data were obtained under program ID P71-506 (PIs: Daniele B. Malesani, Johan P. U. Fynbo, Dong Xu).

The MeerKAT telescope is operated by the South African Radio Astronomy Observatory, which is a facility of the National Research Foundation, an agency of the Department of Science and Innovation. This work has made use of the “MPIfR S-band receiver system,” designed, constructed, and maintained by funding of the MPI für Radioastronomie and the Max Planck Society.

A.M.C. and L.C. acknowledge support from the Irish Research Council Postgraduate Scholarship No. GOIPG/2022/1008. P.G.J. J.S.S., J.Q.V., and M.E.R. are supported by the European Union (ERC, Starstruck, grant No. 101095973; PI: Jonker). Views and opinions expressed are however those of the author(s) only and do not necessarily reflect those of the European Union or the European Research Council Executive Agency. Neither the European Union nor the granting authority can be held responsible for them. B.S. and S.D.V. acknowledge the support of the French Agence Nationale de la Recherche (ANR), under grant ANR-23-CE31-0011 (project PEGaSUS). A.S. acknowledges support by a postdoctoral fellowship from the CNES. J.C.R. acknowledges support from the Northwestern Presidential Fellowship. B.P.G. acknowledges support from STFC grant No. ST/Y002253/1 and the Leverhulme Trust grant No. RPG-2024-117. Dimple acknowledges support from STFC grant No. ST/Y002253/1. M.E.W. is supported by the UKRI Science and Technology Facilities Council (STFC). This work was supported by a research grant (VIL54489) from VILLUM FONDEN. R.S. acknowledges the Leverhulme Trust grant No. RP-2023-240. D.B.M., D.W., and A.S. are funded by the European Union (ERC, HEAVYMETAL, grant No. 101071865). The Cosmic Dawn Center (DAWN) is funded by the Danish National Research Foundation under grant DNR140.

Appendix A Afterglow Modeling

For our modeling, we download the Swift-XRT count-rate light curve and convert to flux density at 1 keV using the spectral parameters reported on the Swift website.⁴⁰ We use the NIR fluxes unsubtracted for host emission and incorporate a constant component at the K band to account for host contamination. Our modeling framework is described in detail elsewhere (T. Laskar et al. 2013, 2014), but, in summary, we use the standard analytical model of J. Granot & R. Sari (2002) with allowance for dust extinction in the Milky Way and in the host galaxy (following a Small Magellanic Cloud dust law), radio scintillation, inverse-Compton cooling, and Klein–Nishina corrections (Y. C. Pei 1992; J. Goodman & R. Narayan 2006; G. A. McCarthy & T. Laskar 2024). The free parameters of our FS model, along with their best-fit values, are the electron energy index (p), the fraction of postshock energy in accelerated electrons (ϵ_e) and in the magnetic field (ϵ_B), $E_{K,iso}$, the density

⁴⁰ We use $\Gamma = 1.6$ and a counts-to-flux conversion factor of 9×10^{-11} erg cm⁻² ct⁻¹. The parameters reported on the website may drift following continued monitoring.

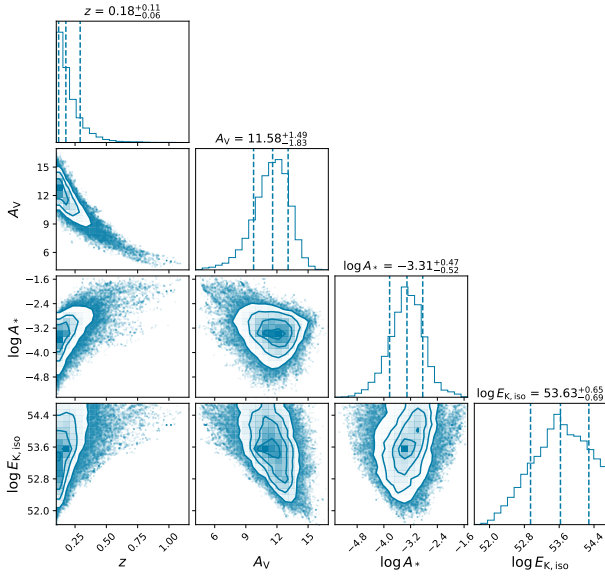


Figure 6. Correlation plots and marginalized posterior density functions for four key free parameters in the afterglow model (Section 5 and Appendix A), demonstrating that low-redshift $z \lesssim 0.3$ and high-extinction ($A_v \gtrsim 10$ mag) models are favored by the data under the modeling constraints employed here.

parameter (A_*) for a wind-like environment, t_{jet} , $F_{\nu, \text{host}, K}$, and the redshift z . We additionally incorporate an RS component with the following fixed locations of the three spectral break frequencies: $\nu_a \approx 2 \times 10^{12}$ Hz (self-absorption), $\nu_m \approx 3 \times 10^{18}$ Hz (peak), and $\nu_c \approx 8 \times 10^{18}$ Hz (cooling), as well as peak flux $F_{\nu, m, \text{RS}} \approx 5 \times 10^4$ mJy, all at a fiducial $\delta t = 10^{-3}$ days, chosen to approximately match the radio spectral energy distributions without overpredicting the near-IR data.

We sample the parameter space using a Markov Chain Monte Carlo method with *emcee* (D. Foreman-Mackey et al. 2013). We run 512 walkers for 2000 steps and discard the first 30 steps as burn-in. We plot correlation contours for four parameters of particular interest in Figure 6. The parameters of the highest-likelihood model are $p \approx 2.2$, $\epsilon_e \approx 0.95$, $\epsilon_B \approx 1 \times 10^{-2}$, $E_{K, \text{iso}} \approx 4 \times 10^{53}$ erg, $A_* \approx 8 \times 10^{-4}$, $t_{\text{jet}} \approx 0.1$ day, $F_{\nu, K, \text{host}} \approx 2.9 \times 10^{-3}$ mJy, and $z \approx 0.16$. For this model (plotted in Figure 5), the FS break frequencies and peak flux density at 1 day are $\nu_a \approx 7 \times 10^5$ Hz, $\nu_c \approx 3 \times 10^{20}$ Hz, $\nu_m \approx 3 \times 10^{13}$ Hz, and $F_{\nu, m, \text{FS}} \approx 0.5$ mJy. The outer break frequencies are unconstrained by the data in this model, resulting in degeneracies between the model parameters; however, these degeneracies are suppressed by the additional requirement of $\epsilon_e + \epsilon_B < 1$, reducing the available parameter space and tightening the posterior in this case. While the data only constrain $t_{\text{jet}} \lesssim 0.5$ day (the first Swift-XRT detection), the smoothing used in the model light curves pushes the best-fit t_{jet} earlier. We infer a very small opening angle, $\theta_{\text{jet}} = 9.7[A_*/E_{K, \text{iso}, 52}(1+z)]^{1/4} \approx 0.4^\circ$, which is lower than inferred for any afterglow previously (T. Laskar et al. 2015), although perhaps not impossible to achieve (e.g., O. S. Salafia et al. 2020); nevertheless, we acknowledge this as a challenge that warrants further investigation beyond the scope of this work. Finally, we note that the RS parameters are simply chosen to roughly match the radio data; a more complete analysis of the RS (and the FS) will require the full multiwavelength (and in particular radio) data set. We defer such analysis to future work.

Appendix B Additional Redshift Constraints

B.1. Host Galaxy

In the absence of an absorption redshift from the afterglow, the most promising route to obtain the distance to GRB 250702B is via the host galaxy. At present, the available X-shooter spectroscopy does not yield any emission lines, and only two photometric bands are available. Hence, neither spectroscopic nor photometric redshift measurements are possible, and no precise redshift can be determined from the host galaxy. However, the relative brightness and extent of the host can be used to place some limits.

In Figure 7, we plot the physical size (in kiloparsecs) and absolute magnitude of the host of GRB 250702B as it would appear at various redshifts from ($0.01 < z < 3$). We also compare to the evolving galaxy size–redshift relationship from K. Ormerod et al. (2024), which demonstrates that galaxies at higher redshift are typically more compact than those locally. We further compare to the host galaxies of GRBs observed with HST in a similar observed band to the observations of GRB 250702B (F160W from J. D. Lyman et al. 2017 compared to the F140W used here). For comparison to galaxy masses, we also include a crude mass conversion based on the *K*-band luminosity (S. Savaglio et al. 2009; K. M. Svensson et al. 2010), and plot the stellar masses and sizes of galaxies studied in the Hubble Frontier Fields (L. Yang et al. 2021). Figure 7 demonstrates that, at low redshift $0.1 < z < 0.5$, the galaxy would be consistent with both the sizes of the galaxy population and the properties of GRB hosts. Beyond $z \sim 0.5$, the GRB 250702B host would be a large and luminous galaxy.

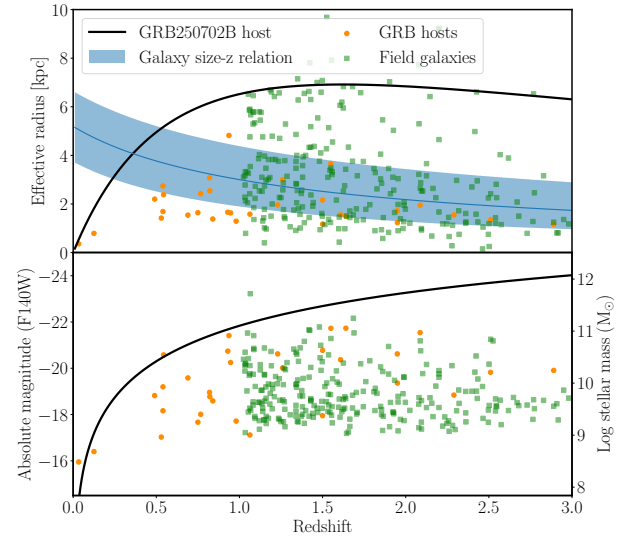


Figure 7. The effective radius (top) and absolute magnitude of the host galaxy of GRB 250702B at various redshifts from $0.1 < z < 3$. The top panel shows how the physical radius would evolve across the redshift range (black line), while the shaded blue region is the galaxy size–redshift relation from K. Ormerod et al. (2024), and the green points a set of direct measurements of high- z ($z > 1$) galaxy sizes (and masses) from the Hubble Frontier Fields (L. Yang et al. 2021). The GRB host population from J. D. Lyman et al. (2017) is also shown. The lower panel shows the absolute magnitude of the host galaxy in the F140W filter, as well as a crude conversion to stellar mass. Both the sizes and luminosities of the host of GRB 250702B would be consistent with the GRB host and field galaxy population at low z , matching particularly well at $z < 0.5$. At higher redshift large, luminous galaxies do occur, but as the intrinsic luminosity of the GRB 250702B host increases with redshift, they become increasingly rare. The host would be unusually luminous beyond $z \sim 1$.








Such galaxies are underrepresented in the host population of the GRB, likely due to metallicity bias (e.g., A. S. Fruchter et al. 2006; D. A. Perley et al. 2016), but do exist in field surveys in reasonable numbers. Indeed, if the progenitor of GRB 250702B is not a collapsar, then the host selection could well differ from that of most GRBs. Beyond $z \sim 1$, the luminosity (and stellar mass) of the galaxy becomes very large, such that few such luminous galaxies are found in deep field surveys at $1 < z < 3$ (e.g., L. Yang et al. 2021; E. Ward et al. 2024), although such galaxies naturally have large radii.

Finally, if we interpret the morphology of the host galaxy as due to the presence of a dust lane, then this lane is apparently resolved at the resolution of the HST IR channel ($\sim 0''.15$). Since such dust structures are typically confined to the disks of galaxies, they are normally only a few hundred parsec across. At $z \sim 1$, $0''.15$ is > 1 kpc, which would suggest an unusual dust structure in this case, but a much more typical dust structure at $z \sim 0.25$ where the resolution element corresponds to 500 pc. Hence, as with our other diagnostics, the host properties would favor, though not conclusively prove, a moderate-redshift scenario ($0.1 < z < 0.5$) for GRB 250702B.

B.2. X-Ray Column

Another constraint on the redshift can be obtained by comparing the X-ray absorbing column density to the optical/near-IR extinction. In the Galaxy, the X-ray absorbing column density, N_{Hx} , is strongly correlated with the dust column (e.g., D. Watson 2011), and is expected to be strongly correlated for most galaxies, as the ISM X-ray absorption is due to metals while dust is strongly correlated with the total metal column density. The ratio is about $N_{\text{Hx}}/A_V \simeq 2 \times 10^{21} \text{ cm}^{-2} \text{ mag}^{-1}$ (e.g., T. Güver & F. Özel 2009; D. Watson 2011; H. Zhu et al. 2017). The extinction and X-ray absorption estimates scale with redshift. For extinction, this is $A_V(z) \simeq A_V(z=0) \times (1+z)^{-1.4}$, depending on the extinction curve. The X-ray absorption scales as $N_{\text{Hx}}(z) \simeq N_{\text{Hx}}(z=0) \times (1+z)^{2.4}$ (S. Campana et al. 2014). These work in opposing directions, such that $\frac{N_{\text{Hx}}(z)/A_V(z)}{N_{\text{Hx}}(z=0)/A_V(z=0)} = (1+z)^{3.8}$. If we assume the ratio $N_{\text{Hx}}(z)/A_V(z) = 2 \times 10^{21} \text{ cm}^{-2} \text{ mag}^{-1}$, then we can infer the approximate redshift: $z = \left(\frac{2 \times 10^{21} \text{ cm}^{-2} \text{ mag}^{-1}}{N_{\text{Hx}}(z=0)/A_V(z=0)} \right)^{\frac{1}{3.8}} - 1$. If $A_V(z)$ is known (e.g., in our case from afterglow modeling), then the corresponding expression is $z = \left(\frac{2 \times 10^{21} \text{ cm}^{-2} \text{ mag}^{-1}}{N_{\text{Hx}}(z=0)/A_V(z)} \right)^{\frac{1}{2.4}} - 1$. In practice, the X-ray absorption-to-extinction ratio and power-law index will have uncertainties, for which we assume 10% and ± 0.1 , respectively.

ORCID iDs

Andrew J. Levan  <https://orcid.org/0000-0001-7821-9369>
 Antonio Martin-Carrillo  <https://orcid.org/0000-0001-5108-0627>
 Tanmoy Laskar  <https://orcid.org/0000-0003-1792-2338>
 Rob A. J. Eyles-Ferris  <https://orcid.org/0000-0002-8775-2365>
 Albert Snenppen  <https://orcid.org/0000-0002-5460-6126>
 Maria Edvige Ravasio  <https://orcid.org/0000-0003-3193-4714>
 Jillian C. Rastinejad  <https://orcid.org/0000-0002-9267-6213>

Joe S. Bright  <https://orcid.org/0000-0002-7735-5796>
 Francesco Carotenuto  <https://orcid.org/0000-0002-0426-3276>
 Ashley A. Chrimes  <https://orcid.org/0000-0001-9842-6808>
 Gregory Corcoran  <https://orcid.org/0009-0009-1573-8300>
 Benjamin P. Gompertz  <https://orcid.org/0000-0002-5826-0548>
 Peter G. Jonker  <https://orcid.org/0000-0001-5679-0695>
 Gavin P. Lamb  <https://orcid.org/0000-0001-5169-4143>
 Daniele B. Malesani  <https://orcid.org/0000-0002-7517-326X>
 Andrea Saccardi  <https://orcid.org/0000-0002-6950-4587>
 Javier Sánchez-Sierras  <https://orcid.org/0000-0003-2276-4231>
 Benjamin Schneider  <https://orcid.org/0000-0003-4876-7756>
 Steve Schulze  <https://orcid.org/0000-0001-6797-1889>
 Nial R. Tanvir  <https://orcid.org/0000-0003-3274-6336>
 Susanna D. Vergani  <https://orcid.org/0000-0001-9398-4907>
 Darach Watson  <https://orcid.org/0000-0002-4465-8264>
 Jie An  <https://orcid.org/0009-0000-5068-3434>
 Franz E. Bauer  <https://orcid.org/0000-0002-8686-8737>
 Sergio Campana  <https://orcid.org/0000-0001-6278-1576>
 Laura Cotter  <https://orcid.org/0000-0002-7910-6646>
 Joyce N. D. van Dalen  <https://orcid.org/0009-0007-6927-7496>
 Valerio D'Elia  <https://orcid.org/0000-0002-7320-5862>
 Massimiliano De Pasquale  <https://orcid.org/0000-0002-4036-7419>
 Antonio de Ugarte Postigo  <https://orcid.org/0000-0001-7717-5085>
 Dimple  <https://orcid.org/0000-0001-9868-9042>
 Dieter H. Hartmann  <https://orcid.org/0000-0002-8028-0991>
 Jens Hjorth  <https://orcid.org/0000-0002-4571-2306>
 Luca Izzo  <https://orcid.org/0000-0001-9695-8472>
 Páll Jakobsson  <https://orcid.org/0000-0002-9404-5650>
 Amit Kumar  <https://orcid.org/0000-0002-4870-9436>
 Andrea Melandri  <https://orcid.org/0000-0002-2810-2143>
 Paul O'Brien  <https://orcid.org/0000-0002-5128-1899>
 Silvia Piranomonte  <https://orcid.org/0000-0002-8875-5453>
 Giovanna Pugliese  <https://orcid.org/0000-0003-3457-9375>
 Jonathan Quirola-Vásquez  <https://orcid.org/0000-0001-8602-4641>
 Rhaana Starling  <https://orcid.org/0000-0001-5803-2038>
 Gianpiero Tagliaferri  <https://orcid.org/0000-0003-0121-0723>
 Dong Xu  <https://orcid.org/0000-0003-3257-9435>
 Makenzie E. Wortley  <https://orcid.org/0009-0009-8473-3407>

References

- Abbott, B. P., Abbott, R., Abbott, T. D., et al. 2017, *PhRvL*, 119, 161101
 Alexander, K. D., Miller-Jones, J., Goodwin, A., et al. 2025, *GCN*, 41059, 1
 Amati, L. 2006, *MNRAS*, 372, 233
 Andreoni, I., Coughlin, M. W., Perley, D. A., et al. 2022, *Natur*, 612, 430
 Atri, P., Rhodes, L., Fender, R., et al. 2025, *GCN*, 41054, 1
 Atteia, J.-L., Bouchet, L., Dezalay, J.-P., et al. 2025, *ApJ*, 980, 241
 Band, D., Matteson, J., Ford, L., et al. 1993, *ApJ*, 413, 281
 Barkov, M. V., & Komisarov, S. S. 2010, *MNRAS*, 401, 1644
 Beniamini, P., Piran, T., & Matsumoto, T. 2023, *MNRAS*, 524, 1386
 Berger, E., Fong, W., & Chornock, R. 2013, *ApJL*, 774, L23
 Bloom, J. S., Giannios, D., Metzger, B. D., et al. 2011, *Sci*, 333, 203

- Bloom, J. S., Kulkarni, S. R., & Djorgovski, S. G. 2002, *AJ*, **123**, 1111
- Bright, A. J., Carotenuto, F., & Jonker, P. G. 2025, GCN, 40985, 1
- Bromberg, O., Nakar, E., Piran, T., & Sari, R. 2013, *ApJ*, **764**, 179
- Brown, G. C., Levan, A. J., Stanway, E. R., et al. 2015, *MNRAS*, **452**, 4297
- Burns, E., Svinkin, D., Fenimore, E., et al. 2023, *ApJL*, **946**, L31
- Burns, E., Svinkin, D., Hurley, K., et al. 2021, *ApJL*, **907**, L28
- Burrows, D. N., Kennea, J. A., Ghisellini, G., et al. 2011, *Natur*, **476**, 421
- Busmann, M., Hall, X. J., O'Connor, B., et al. 2025, GCN, 40949, 1
- Camilo, F., Scholz, P., Serylak, M., et al. 2018, *ApJ*, **856**, 180
- Campana, S., Bernardini, M. G., Braito, V., et al. 2014, *MNRAS*, **441**, 3634
- CASA Team, Bean, B., Bhatnagar, S., et al. 2022, *PASP*, **134**, 114501
- Cenko, S. B., Frail, D. A., Harrison, F. A., et al. 2011, *ApJ*, **732**, 29
- Cenko, S. B., Krimm, H. A., Horesh, A., et al. 2012, *ApJ*, **753**, 77
- Chandra, P., & Frail, D. A. 2012, *ApJ*, **746**, 156
- Cheng, H. Q., Zhao, G. Y., Zhou, C., et al. 2025, GCN, 40906, 1
- Church, R. P., Kim, C., Levan, A. J., & Davies, M. B. 2012, *MNRAS*, **425**, 470
- Cufari, M., Coughlin, E. R., & Nixon, C. J. 2022a, *ApJL*, **929**, L20
- Cufari, M., Coughlin, E. R., & Nixon, C. J. 2022b, *ApJ*, **924**, 34
- Das, K. K., Sharma, K., Karambelkar, V., et al. 2025, GCN, 41044, 1
- deLaunay, J., Ronchini, S., Tohuavavohu, A., et al. 2025, GCN, 40903, 1
- de Mink, S. E., Sana, H., Langer, N., Izzard, R. G., & Schneider, F. R. N. 2014, *ApJ*, **782**, 7
- Dermer, C. D., Hurley, K. C., & Hartmann, D. H. 1991, *ApJ*, **370**, 341
- de Ugarte Postigo, A., Lundgren, A., Martín, S., et al. 2012, *A&A*, **538**, A44
- Duffell, P. C., & MacFadyen, A. I. 2015, *ApJ*, **806**, 205
- Eftekhari, T., & Berger, E. 2017, *ApJ*, **849**, 162
- Eftekhari, T., Tchekhovskoy, A., Alexander, K. D., et al. 2024, *ApJ*, **974**, 149
- Evans, P. A., Beardmore, A. P., Page, K. L., et al. 2007, *A&A*, **469**, 379
- Evans, P. A., Beardmore, A. P., Page, K. L., et al. 2009, *MNRAS*, **397**, 1177
- Evans, P. A., Page, K. L., Beardmore, A. P., et al. 2023, *MNRAS*, **518**, 174
- Evans, P. A., Willingale, R., Osborne, J. P., et al. 2010, *A&A*, **519**, A102
- Foreman-Mackey, D., Hogg, D. W., Lang, D., & Goodman, J. 2013, *PASP*, **125**, 306
- Frederiks, D., Lysenko, A., Ridnaia, A., et al. 2025, GCN, 40914, 1
- Fruchter, A. S., Levan, A. J., Strolger, L., et al. 2006, *Natur*, **441**, 463
- Fryer, C. L., Burns, E., Ho, A. Y. Q., et al. 2025, *ApJ*, **986**, 185
- Fryer, C. L., Woosley, S. E., & Hartmann, D. H. 1999, *ApJ*, **526**, 152
- Ghirlanda, G., Nappo, F., Ghisellini, G., et al. 2018, *A&A*, **609**, A112
- Goodman, J., & Narayan, R. 2006, *ApJ*, **636**, 510
- Granot, J., & Sari, R. 2002, *ApJ*, **568**, 820
- Greiner, J., Mazzali, P. A., Kann, D. A., et al. 2015, *Natur*, **523**, 189
- Güver, T., & Özel, F. 2009, *MNRAS*, **400**, 2050
- Hammerstein, E., Cenko, S. B., Andreoni, I., et al. 2025, arXiv:2506.08250
- Heng, K., Lazzati, D., & Perna, R. 2007, *ApJ*, **662**, 1119
- Hewett, P. C., Warren, S. J., Leggett, S. K., & Hodgkin, S. T. 2006, *MNRAS*, **367**, 454
- Heywood, I. 2020, oxdcat: Semi-automated Imaging of MeerKAT Observations, Astrophysics Source Code Library, ascl:2009.003
- Hills, J. G. 1988, *Natur*, **331**, 687
- Hjorth, J., Sollerman, J., Møller, P., et al. 2003, *Natur*, **423**, 847
- Hua, Y.-L., Geng, J.-J., Wu, X.-F., et al. 2025, GCN, 40943, 1
- Hugo, B. V., Perkins, S., Merry, B., Mauch, T., & Smirnov, O. M. 2022, in ASP Conf. Ser. 532, Astronomical Data Analysis Software and Systems XXX, ed. J. E. Ruiz, F. Pierfederici, & P. Teuben (San Francisco, CA: ASP), 541
- Hurley, K., Boggs, S. E., Smith, D. M., et al. 2005, *Natur*, **434**, 1098
- Irwin, J. A., Brink, T. G., Bregman, J. N., & Roberts, T. P. 2010, *ApJL*, **712**, L1
- Jin, C. C., Li, D. Y., Jiang, N., et al. 2025, arXiv:2501.09580
- Jonas, J. 2018, in Proc. MeerKAT Science: On the Pathway to the SKA, ed. M. Gyssens & J.-L. Rault (Mechelen: International Meteor Organization), 001
- Jonker, P. G., Glennie, A., Heida, M., et al. 2013, *ApJ*, **779**, 14
- Kann, D. A., White, N. E., Ghirlanda, G., et al. 2024, *A&A*, **686**, A56
- Kawakubo, Y., Serino, M., Negoro, H., et al. 2025, GCN, 40910, 1
- Kennea, J. A., Siegel, M. H., Evans, P. A., et al. 2025, GCN, 40919, 1
- King, A. 2022, *MNRAS*, **515**, 4344
- Klose, S. 1998, *ApJ*, **507**, 300
- Kouveliotou, C., Meegan, C. A., Fishman, G. J., et al. 1993, *ApJL*, **413**, L101
- Krolik, J. H., & Piran, T. 2011, *ApJ*, **743**, 134
- Laskar, T., Berger, E., Margutti, R., et al. 2015, *ApJ*, **814**, 1
- Laskar, T., Berger, E., Tanvir, N., et al. 2014, *ApJ*, **781**, 1
- Laskar, T., Berger, E., Zauderer, B. A., et al. 2013, *ApJ*, **776**, 119
- Levan, A. J., Gompertz, B. P., Salafia, O. S., et al. 2024, *Natur*, **626**, 737
- Levan, A. J., Gompertz, B. P., Smith, G. P., et al. 2025a, *RSPTA*, **383**, 20240122
- Levan, A. J., Martin-Carrillo, A., Schneider, B., et al. 2025b, GCN, 40961, 1
- Levan, A. J., Tanvir, N. R., Brown, G. C., et al. 2016, *ApJ*, **819**, 51
- Levan, A. J., Tanvir, N. R., Cenko, S. B., et al. 2011, *Sci*, **333**, 199
- Levan, A. J., Tanvir, N. R., Starling, R. L. C., et al. 2014, *ApJ*, **781**, 13
- Lloyd-Ronning, N. M., Dolence, J. C., & Fryer, C. L. 2016, *MNRAS*, **461**, 1045
- Lucas, P. W., Hoare, M. G., Longmore, A., et al. 2008, *MNRAS*, **391**, 136
- Lyman, J. D., Levan, A. J., Tanvir, N. R., et al. 2017, *MNRAS*, **467**, 1795
- MacLeod, M., Guillochon, J., Ramirez-Ruiz, E., Kasen, D., & Rosswog, S. 2016, *ApJ*, **819**, 3
- Madau, P., Blandford, R. D., & Rees, M. J. 2000, *ApJ*, **541**, 712
- Malesani, D. B., Levan, A. J., Izzo, L., et al. 2023, arXiv:2302.07891
- Mangano, V., Burrows, D. N., Sbarufatti, B., & Cannizzo, J. K. 2016, *ApJ*, **817**, 103
- Martin-Carrillo, A., Levan, A. J., Schneider, B., et al. 2025, GCN, 40924, 1
- McCarthy, G. A., & Laskar, T. 2024, *ApJ*, **970**, 135
- Melandri, A., Sbarufatti, B., D'Avanzo, P., et al. 2012, *MNRAS*, **421**, 1265
- Mereghetti, S., Rigoselli, M., Salvaterra, R., et al. 2024, *Natur*, **629**, 58
- Metzger, B. D., Margalit, B., Kasen, D., & Quataert, E. 2015, *MNRAS*, **454**, 3311
- Miniutti, G., Saxton, R. D., Giustini, M., et al. 2019, *Natur*, **573**, 381
- Moran, J. A., & Reichart, D. E. 2005, *ApJ*, **632**, 438
- Neights, E., Roberts, O. J., Burns, E., Veres, P., & Fermi-GBM Team 2025a, GCN, 40891, 1
- Neights, E., Roberts, O. J., Burns, E., et al. 2025b, GCN, 40931, 1
- Nixon, C. J., Coughlin, E. R., & Miles, P. R. 2021, *ApJ*, **922**, 168
- Nomoto, K., & Kondo, Y. 1991, *ApJL*, **367**, L19
- O'Connor, B., Pasham, D., Andreoni, I., & Hare, J. 2025, GCN, 41014, 1
- Offringa, A. R., McKinley, B., Hurley-Walker, N., et al. 2014, *MNRAS*, **444**, 606
- Ormerod, K., Conselice, C. J., Adams, N. J., et al. 2024, *MNRAS*, **527**, 6110
- Paczynski, B. 1986, *ApJL*, **308**, L43
- Pasham, D. R., Cenko, S. B., Levan, A. J., et al. 2015, *ApJ*, **805**, 68
- Pasham, D. R., Lucchini, M., Laskar, T., et al. 2023, *NatAs*, **7**, 88
- Pei, Y. C. 1992, *ApJ*, **395**, 130
- Peng, C. Y., Ho, L. C., Impey, C. D., & Rix, H.-W. 2010, *AJ*, **139**, 2097
- Perets, H. B., Li, Z., Lombardi, J. C., Jr., & Milcarek, S. R., Jr. 2016, *ApJ*, **823**, 113
- Pérez-García, I., Castro-Tirado, A. J., Caballero-García, M. D., et al. 2025, GCN, 40929, 1
- Perley, D. A., Levan, A. J., Tanvir, N. R., et al. 2013, *ApJ*, **778**, 128
- Perley, D. A., Tanvir, N. R., Hjorth, J., et al. 2016, *ApJ*, **817**, 8
- Perna, R., Armitage, P. J., & Zhang, B. 2006, *ApJL*, **636**, L29
- Planck Collaboration, Aghanim, N., Akrami, Y., et al. 2020, *A&A*, **641**, A6
- Portegies Zwart, S. F., Baumgardt, H., Hut, P., Makino, J., & McMillan, S. L. W. 2004, *Natur*, **428**, 724
- Quataert, E., & Kasen, D. 2012, *MNRAS*, **419**, L1
- Rastinejad, J. C., Gompertz, B. P., Levan, A. J., et al. 2022, *Natur*, **612**, 223
- Rees, M. J. 1988, *Natur*, **333**, 523
- Rhodes, L., Margalit, B., Bright, J. S., et al. 2025, arXiv:2506.13618
- Salafia, O. S., Barbieri, C., Ascenzi, S., & Toffano, M. 2020, *A&A*, **636**, A105
- Savaglio, S., Glazebrook, K., & Le Borgne, D. 2009, *ApJ*, **691**, 182
- Schady, P., Page, M. J., Oates, S. R., et al. 2010, *MNRAS*, **401**, 2773
- Schlaflly, E. F., & Finkbeiner, D. P. 2011, *ApJ*, **737**, 103
- Schneider, B., Le Floc'h, E., Arabsalmani, M., Vergani, S. D., & Palmerio, J. T. 2022, *A&A*, **666**, A14
- Schröder, S. L., MacLeod, M., Loeb, A., Vigna-Gómez, A., & Mandel, I. 2020, *ApJ*, **892**, 13
- Schroeder, G., Laskar, T., Fong, W.-f., et al. 2022, *ApJ*, **940**, 53
- Schulze, S., Malesani, D., Cucchiara, A., et al. 2014, *A&A*, **566**, A102
- Selsing, J., Malesani, D., Goldoni, P., et al. 2019, *A&A*, **623**, A92
- Sfaradi, A. I., Margutti, R., Farah, W., et al. 2025a, GCN, 40979, 1
- Sfaradi, A. I., Yao, Y., Sears, H., et al. 2025b, GCN, 41053, 1
- Shao, L., & Dai, Z. G. 2007, *ApJ*, **660**, 1319
- Shao, L., Dai, Z. G., & Mirabal, N. 2008, *ApJ*, **675**, 507
- Stanek, K. Z., Matheson, T., Garnavich, P. M., et al. 2003, *ApJL*, **591**, L17
- Suwa, Y., & Ioka, K. 2011, *ApJ*, **726**, 107
- Svensson, K. M., Levan, A. J., Tanvir, N. R., Fruchter, A. S., & Strolger, L. G. 2010, *MNRAS*, **405**, 57
- Svensson, K. M., Levan, A. J., Tanvir, N. R., et al. 2012, *MNRAS*, **421**, 25
- SVOM/GRM Team, Wang, C.-W., Zheng, S.-J., et al. 2025, GCN, 40923, 1
- Tanvir, N. R., Levan, A. J., Fruchter, A. S., et al. 2013, *Natur*, **500**, 547
- Teboul, O., & Metzger, B. D. 2023, *ApJL*, **957**, L9
- Tetarenko, A. J., Bright, J., Bower, G., & Graves, S. 2025, GCN, 41061, 1

- Tohuvavohu, A., Kennea, J. A., DeLaunay, J., et al. 2020, [ApJ](#), **900**, 35
- Trigg, A. C., Stewart, R., Van Kooten, A., et al. 2025, [A&A](#), **694**, A323
- Troja, E., Fryer, C. L., O'Connor, B., et al. 2022, [Natur](#), **612**, 228
- Tsvetkova, A., Frederiks, D., Golenetskii, S., et al. 2017, [ApJ](#), **850**, 161
- van Eerten, H. J. 2014, [MNRAS](#), **445**, 2414
- van Putten, M. H. P. M. 1999, [Sci](#), **284**, 115
- Vernet, J., Dekker, H., D'Odorico, S., et al. 2011, [A&A](#), **536**, A105
- Wang, C.-W., Xiong, S.-L. & Gecam Team 2025, GCN, **40922**, 1
- Ward, E., de la Vega, A., Mobasher, B., et al. 2024, [ApJ](#), **962**, 176
- Watson, D. 2011, [A&A](#), **533**, A16
- Watson, D., Zafar, T., Andersen, A. C., et al. 2013, [ApJ](#), **768**, 23
- Windhorst, R. A., Cohen, S. H., Jansen, R. A., et al. 2023, [AJ](#), **165**, 13
- Woosley, S. E., Heger, A., & Weaver, T. A. 2002, [RvMP](#), **74**, 1015
- Yang, J., Ai, S., Zhang, B.-B., et al. 2022, [Natur](#), **612**, 232
- Yang, L., Roberts-Borsani, G., Treu, T., et al. 2021, [MNRAS](#), **501**, 1028
- Yang, Y.-H., Troja, E., O'Connor, B., et al. 2024, [Natur](#), **626**, 742
- Zauderer, B. A., Berger, E., Margutti, R., et al. 2013, [ApJ](#), **767**, 152
- Zhu, H., Tian, W., Li, A., & Zhang, M. 2017, [MNRAS](#), **471**, 3494